Vehviläinen, T.T.; Ganchenkova, M.G.; Nieminen, R.M.

Nanoporous carbon structures based on C20

Published in:
Physical Review B

DOI:
10.1103/PhysRevB.84.125444

Published: 01/01/2011

Document Version
Publisher's PDF, also known as Version of record

Nanoporous carbon structures based on C_{20}

T. T. Vehviläinen,* M. G. Ganchenkova, and R. M. Nieminen
COMP/Department of Applied Physics, School of Science, Aalto University, P.O. Box 11100, FI-00076 Aalto, Espoo, Finland
(Received 28 February 2011; revised manuscript received 29 June 2011; published 28 September 2011)

In this paper, we present computational results for C_{20} based solids. We propose structures that are shown to be energetically more favorable and stable than previously suggested structures. The so-called quasigraphite phase and base-centered-monoclinic type structures are found to be the energetically most favorable. The molecular-dynamics stability of suggested structures was studied via constant-temperature and constant-pressure techniques and by examining phonon dispersion curves. All the predicted structures demonstrate high stability with respect to temperature and external load. By changing the geometry, the electronic properties can be varied from metallic to insulating.

DOI: 10.1103/PhysRevB.84.125444 PACS number(s): 81.05.U−, 78.30.Na, 62.20.−x, 31.15.A−

I. INTRODUCTION

Porous carbon structures, especially zeolite-like carbon materials have been shown to have very high hydrogen storage capacity, which is reversible up to 8.33 wt%.[1] This uptake capacity is one of the highest reported for carbon nanomaterials, and therefore makes similar porous carbon structures promising for hydrogen storage applications. In addition to hydrogen storage,[2–4] fullerene-based structures are possible candidates for superconductors,[5] strong lightweight materials, quantum dots,[6,7] and biological applications.[8,9]

It has been shown that zeolites, which are aluminosilicate minerals and have a microporous structure, can be used as templates for nanostructures where carbon fills the pores and forms three-dimensional networks.[10,11] After the synthesis of the carbon nanostructure, the zeolite template is removed by washing the structure using hydrofluoric acid.[1,11] The resulting material is expected to have pores in original template areas and carbon networks inside original pores, resulting in structural pore ordering similar to that of the zeolite.[1] The solids formed when fullerene molecules[12] form three-dimensional (3D) lattices, have similar porous geometry compared to structures synthetized using zeolite templates. Therefore fullerene solids can serve as excellent model systems for nanotemplated porous carbon nanostructures synthesised in experiments.

So far, mostly C_{60}-based polymers and solids have been studied, both experimentally and theoretically.[13,14] However, the recent synthesis of a broad variety of fullerene cages has opened perspectives to the creation of other kinds of solid structures with different fullerenes as building blocks. We have chosen the smallest fullerene C_{20} as a building block for solid structures. This fullerene consists of 12 pentagons and no hexagons, while in other fullerenes there are also hexagons in the structure. The extreme curvature of the cage surface makes the dihedral angles between bonds (108°) more appropriate to sp^3 hybridization (109.5°) than sp^2, although the C_{20} molecule exhibits sp^2 hybridization. Therefore it can be expected that C_{20} changes hybridization type especially easily, which is a prerequisite for chemical bonding between fullerenes during polymerization process and should manifest extreme reactivity and easy compound formation. However, so far, there have been only two succesfull attempts where three-dimensional C_{20}-based solid has been experimentally produced.[15–17] In Ref. 15, based on the comparison of computational and experimental Raman and IR spectra, Iqbal *et al.* have shown that the best fit to the experimental data is demonstrated by a face-centered cubic C_{22} structure, where C_{20} molecules are located on face-centered cubic lattice sites and are bound by two additional C atoms. Whereas Wang *et al.*[17] managed to synthesize a small amount of hexagonal C_{20} solid using ion beam irradiation method. According to computational studies, other stable 3D solid structures might exist, including simple cubic (sc),[5,18,19] face-centered cubic (fcc),[18,19] and body-centered cubic (bcc)[18–20] phases.

In this article, we propose, based on density-functional-theory calculations, a number of stable C_{20}-based structures. Among these structures are both those described earlier[5,18,20] and those which to our knowledge have not been considered before. Moreover, the structures proposed in this work are energetically the most favorable and stable as compared to previously suggested ones.[5,18,20] The electronic structure, stability, and elastic and vibrational properties of the considered structures are also reported in this paper.

II. COMPUTATIONAL DETAILS

The calculations have been performed using the plane-wave basis VASP code[21,22] implementing the spin-polarized density-functional theory (DFT) and the generalized gradient approximation (GGA) of Perdew and Wang known as PW91.[23] In order to describe the carbon ion core electrons, the projector augmented wave (PAW) potential[24,25] was used. Periodic boundary conditions were used in order to represent C_{20} solids. A kinetic energy cutoff of 400 eV and $6 \times 6 \times 6$ Brillouin-zone sampling were used. These values provide the convergence of the supercell total energy within 10 meV. The relaxations of atomic positions and lattice parameters were performed with molecular-statics methods and the conjugate-gradient algorithm. In order to reproduce different C_{20} structures, the supercell shape was adjusted so that the cell repetition due to periodic boundary conditions would provide the desired overall lattice symmetry. The supercell size was chosen initially so large that the intermolecular separation would suffice to prevent the interaction between the molecule and its periodic images. Then the supercell was gradually decreased until the molecules bonded to each other, forming two- or three-dimensional structures. After the first energy minimum was reached, the cell compression was further

continued in order to study the possible pressure-induced phase transformations of the structure. For this purpose, both isotropic and anisotropic compressions were used. In this way, we have systematically studied the most reasonable structures, which can be created using a 20-atom supercell.

For molecular dynamics simulations and stability studies we used the CPMD[26,27] code, where the Parrinello-Rahman constant-pressure constant-temperature technique and the DFT-GGA approximation are implemented. The size of the supercell for stability studies was 160 atoms and the Brillouin-zone sampling was done with the Γ point.

Phonon-related properties were calculated using the ABINIT[28] code with the local-density approximation (LDA) and density-functional perturbation theory with a $4 \times 4 \times 4$ grid for special high-symmetry q points and a 680-eV kinetic energy cutoff for plane waves.

Some of the studied solids have graphitelike layered structure. In this case, the account of van der Waals (vdW) interactions becomes crucial. In order to take the vdW interaction into account, we have used the empirical damped dispersion model, as described by M. Elstner *et al.*[29] and having the same form as constructed by Mooij *et al.*[30,31] This empirical model allows the estimation of the vdW energy, which is added to the standard DFT energy to obtain total energy of the electron-ion system

$$E_{\mathrm{vdW}} = \sum_{ij} \frac{C_6^{\alpha\beta}}{R_{ij}^{\alpha\beta 6}} \left\{ 1 - \exp\left[-d \left(\frac{R_{ij}^{\alpha\beta}}{R_0^{\alpha\beta}} \right)^7 \right] \right\}^4 . \qquad (1)$$

In this formula, $C_6^{\alpha\beta}$ is the diatomic vdW force coefficient, $R_0^{\alpha\beta}$ is the sum of vdW radii of two interacting atoms, $R_{ij}^{\alpha\beta}$ is the distance between atoms and d is the damping coefficient. The total energy of the electron-ion system is $E_{\mathrm{total}} = E_{\mathrm{DFT}} + E_{\mathrm{vdW}}$. The model ensures that bonded interactions are not doubly counted, because the vdW correction drops to zero when the distance between atoms is less than 3 Å. In the current calculations, we used the set of model parameters obtained by Williams and Malhotra[32] using PBE and BLYP functionals and the vdW corection is used to determine layer-layer distances, bulk moduli and elastic constants only for layered materials. Based on our calculations, neglecting vdW corrections for the other 3D structures does not have a significant effect on the results.

The applicability of the method was tested for the graphite interplane distance optimization. The obtained results show that the measured interplane distances and those calculated with vdW correction, i.e., 3.35 and 3.1 Å, respectively, are in reasonable agreement. The calculated c_{33} elastic constant value of 49 GPa for graphite also reproduces reasonably well the known experimental value of 36 GPa.[33] Comparing to the van der Waals density functional calculations,[34] which give 3.76 Å for the interplane distance and 13 GPa for c_{33} elastic constant, empirical model used in this study seems to give better agreement with experimental values for both lattice and elastic constants.

TABLE I. Energies and lattice parameters for studied polymers with well-known carbon structures. Energies are given without vdW energy taken into account.

Structure	E/atom (eV)	E/atom[18] (eV)	El. prop.	Lattice vectors	Bond lengths (Å)
C-atom	−1.270	...	...	...	...
Diamond	−9.10	−9.22	I, $E_{\mathrm{gap}} = 5.6$ eV	$a = 3.573$ Å	1.54
Graphite	−9.25	−9.24	M	$a = b = 2.46$ Å, $c = 6.2$ Å	1.42
C_{20} molecule	−8.07	−8.01	...	-	1.45
C_{20} sc_{open}	−8.49	−8.48	M	$a = 5.45$ Å	1.42, 1.46
C_{20} sc_{closed}	−8.36	...	S, $E_{\mathrm{gap}} = 1.0$ eV	$a = 6.06$ Å, $b = 6.48$ Å $c = 6.48$ Å	1.38, 1.42, 1.33, 1.48
C_{20} bcm_{closed}	−8.56	−8.56	S, $E_{\mathrm{gap}} = 1.4$ eV	$a_1 = (4.28, 3.81, -0.07)$ Å $a_2 = (-0.07, 3.81, 4.28)$ Å $a_3 = (4.21, 0.00, 4.22)$ Å	1.29, 1.44, 1.50, 1.54 1.61, 1.62, 1.64, 1.69
C_{20} bcm_{open}	−8.79	...	S, $E_{\mathrm{gap}} = 1.5$ eV	$a_1 = (4.31, 4.54, 0.32)$ Å $a_2 = (0.32, 4.54, 4.31)$ Å $a_3 = (3.98, 0.65, 3.98)$ Å	1.34, 1.50, 1.53, 1.54 1.56, 1.57
C_{20} bcc	−8.51	...	S, $E_{\mathrm{gap}} = 2.32$ eV	$a_1 = (-3.37, 3.37, 3.37)$ Å $a_2 = (3.37, -3.37, 3.37)$ Å $a_3 = (3.37, 3.37, -3.37)$ Å	1.34, 1.54
C_{20} hcp	−8.49	...	M	$a_1 = (2.86, 5.57, 0.00)$ Å $a_2 = (2.86 - 5.57, 0.00)$ Å $a_3 = (0.00, 0.00, 6.2)$ Å	1.34, 1.39, 1.41 1.47, 1.50
C_{20} qgp	−8.91	...	M	$a = 4.91$ Å, $b = 5.36$ Å $c = 6.0$ Å	1.41, 1.46, 1.51, 1.55
C_{22} fcc	−8.56	...	S, $E_{\mathrm{gap}} = 2.57$ eV	$a_1 = (0.00, 4.38, 4.38)$ Å $a_2 = (4.38, 0.00, 4.38)$ Å $a_3 = (4.38, 4.38, 0.00)$ Å	1.35, 1.54, 1.56

III. RESULTS AND DISCUSSION

A. Atomic structure

We have systematically created various phases of C_{20} solids as described in Sec. II. First, we focus on base-centered monoclinic (bcm) structures, which are found to be energetically the most favorable ones among typical lattice symmetries, see Table I. Different bcm structures can be created using initial bcm symmetry by variation of mutual orientation of C_{20} molecules constituting the lattice and applying different strains to the structure. In this paper we present two C_{20} bcm solid structures (see Fig. 1), which are called here bcm_{open} and bcm_{closed}. Notations *open* and *closed* refer to the structure of the fullerene cage after the polymerization process. In the *open* structure bonds are broken, opening the cage, while in the *closed* structure there is only bond formation and all bonds in the original fullerene remain intact. The bcm_{closed} structure has been proposed earlier by Okada.[20] However, another bcm-type structure, predicted in this work, turned out to be pronouncedly more favorable, being characterized by the energy of -8.79 eV/atom, as compared to -8.56 eV/atom for bcm_{closed}.[20] In the bcm_{closed} structure, almost all carbon atoms are sp^3 hybridized, while only four atoms remain sp^2 hybridized. All the bonds of the fullerene cage remain unbroken and the cage is closed. However, this is not the case for the bcm_{open} structure, where two bonds of the fullerene cage are broken, which leads to the formation of four new bonds between neighboring molecules and to cage opening. Each carbon atom of the fullerene cage takes part in the bonding. Carbon atoms with broken bonds form new bonds with neighboring fullerenes and remain sp^2 hybridized, while the others become sp^3 hybridized during the polymerization process. Also, as can be seen in Fig. 1, the cage constituting the bcm_{open} solid structure is slightly inclined compared to the bcm_{closed} structure.

The C_{22} fcc structure, which we have reproduced in our studies, is also one of the most interesting structures since it is claimed to be synthetized in experiments.[15,16] In this structure, the C_{20} cages are interlinked together by two interstitial carbon atoms per unit cell. These interstitial carbon atoms and eight atoms in the fullerene cage are sp^3 hybridized while 12 atoms remain sp^2 hybridized. The calculated bond lengths are in agreement with 1.346, 1.517, and 1.531 Å of Iqbal *et al.*, see Table I.

TABLE II. Elastic properties of studied polymers. B^a is bulk modulus calculated using Murnaghan equation of state $E(V) = B^a V/[B^{a'}(B^{a'}-1)][B^{a'}(1-V_0/V)+(V_0/V)^{B^{a'}}-1]$, B^b is bulk modulus calculated using elastic constants $B^b = 1/9(c_{11}+c_{22}+c_{33})+2/9(c_{13}+c_{23}+c_{13})$.

Structure	c_{11}	c_{22}	c_{33}	c_{44}	c_{66}	c_{12}	c_{23}	B^a	B^b
Diamond	1085	...	...	569	...	140	...	447	455
Graphite	1058	...	49	...	...	...	...	34	...
C_{20} sc_{open}	468	...	...	41	...	134	...	247	245
C_{20} sc_{closed}	221	607	20–30	...	67	110	...	15–20	...
C_{20} bcm_{closed}	723	...	581	207	304	108	179	286	312
C_{20} bcm_{open}	753	...	863	324	431	111	211	345	359
C_{20} bcc	375	...	...	165	...	106	...	190	195
C_{20} hcp	633	300	20–35	...	17	49	...	20–30	...
C_{20} qgp	1050	636	48	...	340	90	...	50	...
C_{22} fcc	447	...	...	218	...	109	...	214	221

Under isotropic compression a phase transformation in the sc_{closed} (see Fig. 2) polymer structure was found to take place when the pressure reached the value of 30 GPa. According to the general scheme described above, the fullerene cages are initially packed in a simple cubic lattice, facing each other with parallel edges. Gradual isotropic compression of this system eventually results in the equilibrium layered sc_{closed} structure. If, however, the hydrostatic compression is continued, another phase transformation takes place and a new high-pressure phase, the quasigraphite phase qgp,[35] is formed. The structure of the qgp can be described as an arrangement of small

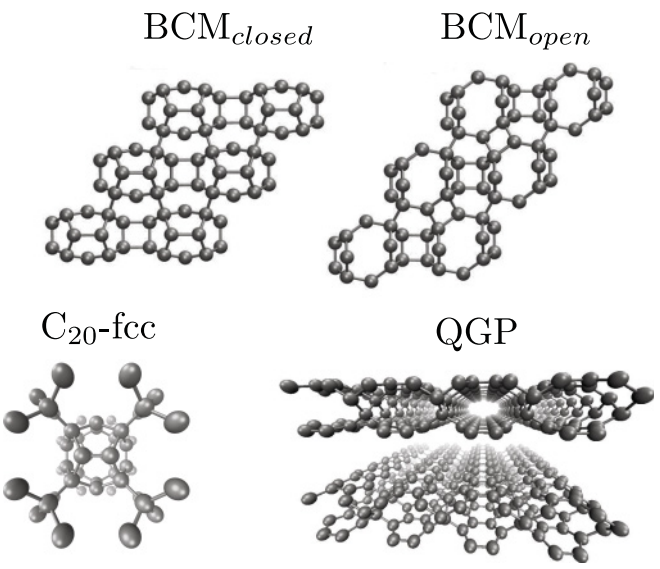

FIG. 1. Geometry of C_{20} bcm-type, qgp, and C_{22}-fcc structures.

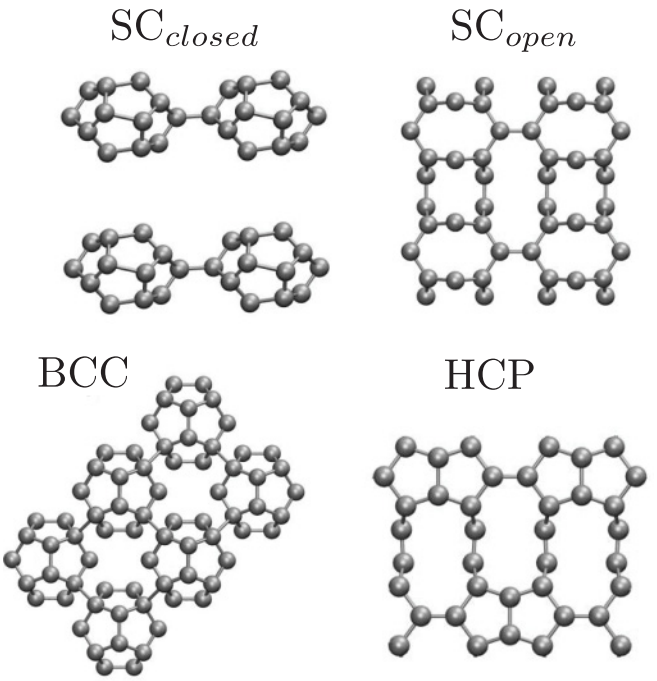

FIG. 2. Geometry of C_{20} sc-type, bcc, and hcp structures.

nanotubes welded together forming planar layers, which are stacked in a graphitelike manner (see Fig. 1). Based on the surface geometry of the tubes, the qgp can be regarded as armchair structure. Due to the welding, tubes are not circular but rather ellipsoids where the minor and major radii are $a = 3.0$ Å and $b = 5.4$ Å, respectively. The atoms that provide nanotube welding manifest the sp^3 hybridization, while other atoms constituting nanotubes have sp^2 hybridization. The distance between the qgp planes is also similar to that in graphite and equals to 3.0 Å. The energy of the qgp structure is −8.91 eV/atom, which is not only more favorable than the intermediate sc structure, but turns out to show the largest cohesive energy among all the equilibrium 3D solids based on the C_{20} fullerene (see Table I). In our procedure of creating solids, the transition is induced exclusively by application of pressure, without any assistance of temperature since the temperature is always zero for the molecular-statics relaxation used here.

The least favorable structures are bcc and hcp structures with energies −8.51 eV and −8.49 eV, respectively. During the polymerization of the bcc phase, eight carbon atoms form bonds with neighboring fullerene and change hybridization to sp^3. While all the original bonds remain unbroken during the synthesis of the bcc phase, this is not the case for hcp phase, where four bonds are broken. However, all atoms of the hcp structure remain sp^2 hybridized.

No magnetic moments were observed in the calculations for any structure.

B. Elastic and electronic properties

Appropriate strains where applied to the equilibrium structures and the observed cell changes and energies were used to calculate elastic constants of the solids. For this purpose the procedure described by Ravindran *et al.*[36] was used. The bulk modulus was calculated both directly from the calculated elastic constants and using the Murnaghan equation of state.[37] The results are summarized in Table II. Both procedures for the bulk modulus calculation give very similar results, confirming the accuracy of the methods. The

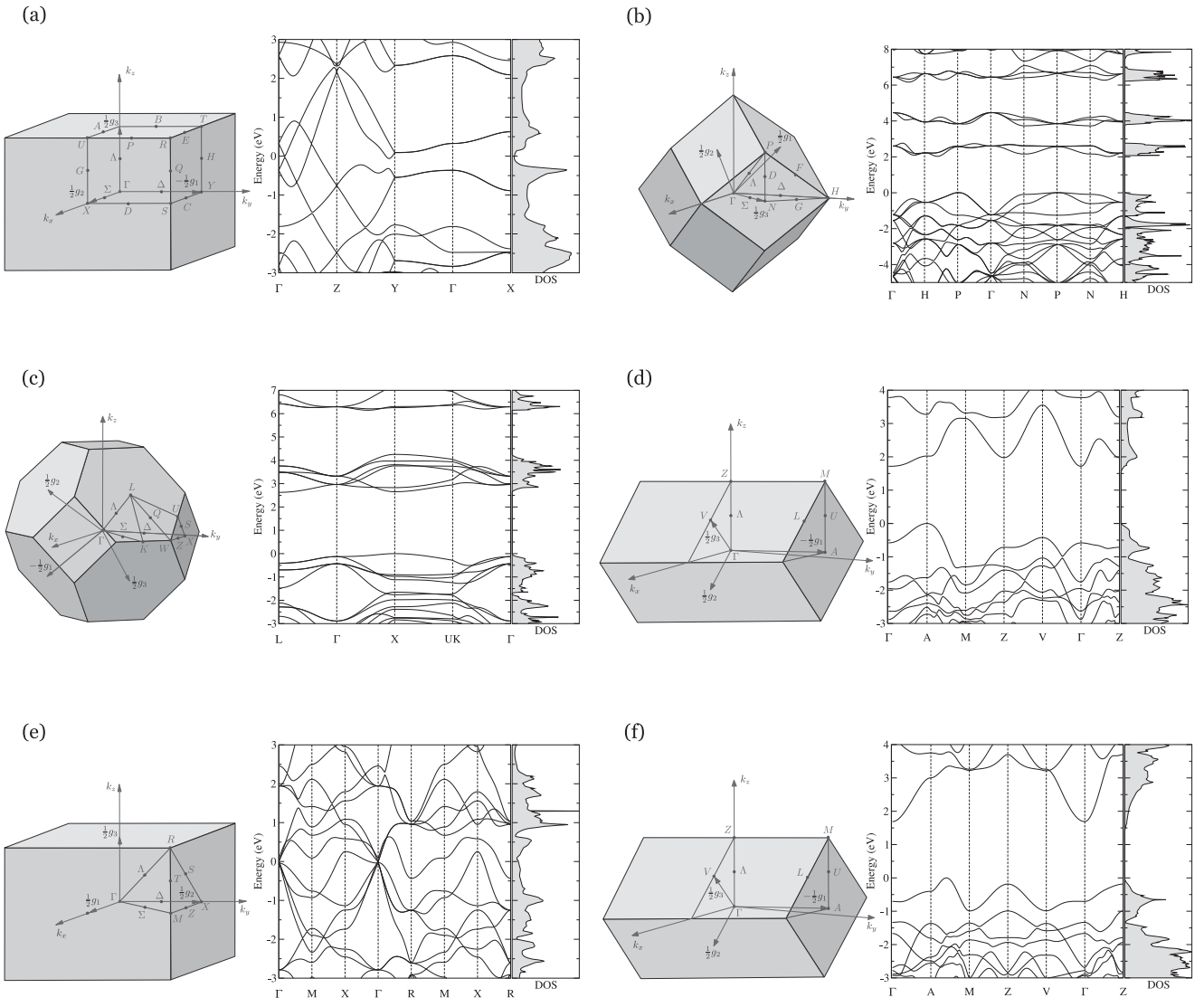

FIG. 3. Band structure plots for energetically most favorable structures: (a) qgp, (b) bcc, (c) fcc-22, (d) bcm_{open}, (e) sc, and (f) bcm_{closed}

results show, in particular, that elastic constants for the fcc structures are large and the structures are, therefore, very rigid, which correlates with the large number of sp^3 hybridized carbon atoms. The bulk modulus of fcc structures is also large, though not as large as that for diamond. The calculated bulk moduli for the layered structures are quite small compared to three-dimensional polymers, which results from the weak van der Waals interaction between the planes. In particular, the elastic constants and the bulk modulus of the qgp structure (50 GPa in Table II) are about the same as for graphite (bulk modulus is 34 GPa in Table II). Calculated values for graphite and diamond are in excellent agreement with experimental results.[33,38]

The results of the electronic structure calculations for all the found polymer structures are summarized in Table I and figures in Ref. 3, where the density of states and band structure plots are presented. Metallic conductivity is observed for qgp, hcp, and sc_{open} structures. The 3D structures are semiconducting except sc_{open}, which is metallic. The band-gap values for semiconductor solids vary from 1.4 (for bcm_{closed}) to 2.57 eV (for C_{22} fcc). Our results are in good agreement with the calculations by Chen[18] for the bcm_{closed} structure and by Miyamoto[5] for the sc_{open} structure. The calculated band gap value for C_{22} fcc is slightly larger compared to the value 2.47 eV calculated in a previous study[15] using LDA, which is known to underestimate the band gap. Band structure plots indicate a direct band gap for the fcc_{22} structure, while the others are indirect band gap semiconductors, see Fig. 3.

Let us now focus on the electronic properties of the qgp structure, which is the energetically most favorable polymer in our studies. This structure manifests metallic properties along the tube axis but no metallic conductivity in in-plane (Γ-X) and perpendicular (Y-Γ) directions (see the band structure and electronic DOS shown in Ref. 35). In contrast to the electronic structure of graphite, there are two well-localized states in the (Γ-X) and (Y-Γ) directions seen in the band gap. In order to excite an electron from the lowest of these localized states, which are fully occupied, to the next empty level one needs only 0.69 and 0.40 eV in (Γ-X) and (Y-Γ) directions, respectively. This electronic band property can possibly be used in applications that require photons with high frequency.

C. Stability

The stability of the considered polymers was studied using the Parrinello-Rahman molecular dynamics (MD) NPT technique implemented in the CPMD code. Both isotropic and anisotropic strains were considered. The performed molecular dynamics calculations showed that all the structures sustain pressures up to 20 GPa at temperatures below 1000 K. However, at higher pressures phase transformations can occur, especially when the pressure is rapidly increased. Structures that are energetically less favorable, like sc structures, undergo phase transformation much easier than fcc or qgp structures. For example, the qgp structure endures pressures up to 50 GPa without any phase transformation, while sc_{closed} splits to graphitelike planes already at 30 GPa. The high-pressure phase for the qgp structure was found to be an amorphous-diamond phase.

D. Vibrational properties

In addition to the MD stability calculations, the nature of phonon vibrational modes can be used to study the stability of the structures. Absence of zero-mode components in the calculated phonon dispersion spectrum is strong evidence for the stability of a structure. A set of dispersion curves for selected structures is shown in Fig. 4. For the C_{22}-fcc structure, the calculated dispersion relation is in good agreement with calculations by Spagnolatti *et al.*[39] The phonon dispersion curves were calculated using finite differences and the *ab initio* perturbation theory approach implemented in the ABINIT[28] code with LDA approximation. In order to estimate the sensitivity of the calculated frequencies to the choice of the exchange-correlation approximation and the code used, the phonon modes were also calculated using both LDA and GGA approximations and VASP. In all tested cases, GGA gives approximately 50 cm^{-1} lower frequencies than LDA, which correlates with the known fact that LDA overestimates interatomic binding, whereas GGA underestimates it. With LDA, VASP gives the same results as ABINIT.

Raman spectroscopy provides another fingerprint by which a structure can be identified, since vibrational information is very sensitive to the spatial disposition of chemical bonds that is unique for each structure. We have also calculated Raman spectra for all the structures, which can be used by

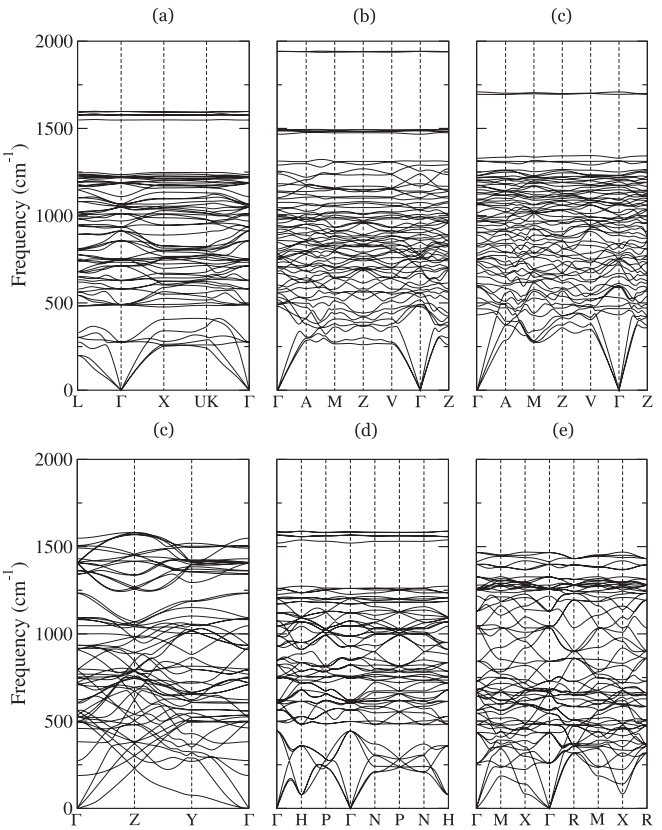

FIG. 4. Calculated dispersion relations for (a) fcc-22 (b) bcm_{closed}, (c) bcm_{open}, (d) qgp (e) bcc, and (f) sc_{open} structures.

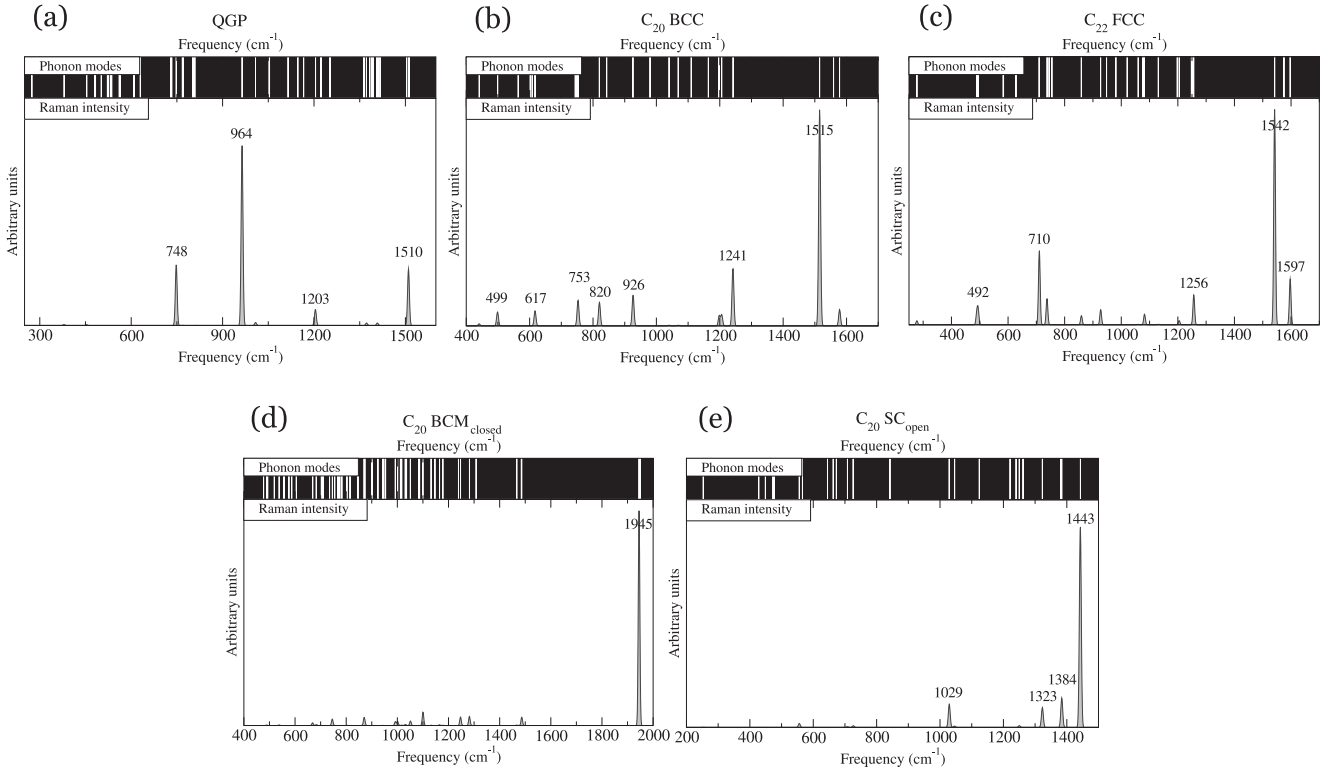

FIG. 5. Calculated Raman spectra for (a) qgp, (b) bcc, (c) fcc-22, (d) bcm_{closed}, and (e) sc_{open} structures.

experimentalists for identification of structures synthetized in experiments. Raman intensities are calculated within the LDA approximation using ABINIT. Linear-response calculations give the Raman susceptibility tensor R, whose elements are derivatives of polarizability. The intensity of a phonon mode is proportional to the largest eigenvalue of R^*R. A mode is Raman active only if the motion occurs with a changing polarizability. At some distance Δr away from the equilibrium structure the polarization α is given by

$$\alpha \approx \alpha_0 + \frac{\partial \alpha}{\partial r}\Delta r, \tag{2}$$

where the term $\partial\alpha/\partial r$ is the change in polarizability with change in a nuclear position. If the derivate is zero, no Raman scattering occurs. In-depth computational details and implementation of the method in ABINIT code can be found in the review article by Baroni *et al.*[40] and the articles by Gonze *et al.*[41–43]

So far, only one experimental Raman spectrum for the C_{20} solid structure has been measured.[15] This spectrum is claimed to belong to the C_{22} structure, although the fit between experimental and computational data is not perfect. The calculated Raman spectra for solids studied in this work are presented in Fig. 5. For the C_{22} structure, the calculated Raman spectrum shows features similar to those calculated by Iqbal *et al.*[15] The most dominant peak positions at 1561, 1506, 729, 697, and 488 cm^{-1} and their intensities calculated in Ref. 15 are in agreement with our calculations, see Fig. 5(c). At the same time, our calculations give a better agreement with experimental peak positions for the two main peaks located at 1585 and 1615 cm^{-1}, though their intensities differ significantly from the measured ones.

In the qgp, C_{20} bcc, C_{20} sc_{open}, and C_{22} fcc spectra we can identify a strong G band located near 1500 cm^{-1}, which is split into several low-intensity peaks. This feature is similar to the G band in graphene (1580 cm^{-1}) and carbon nanotubes, where the G band is split into many features around 1582 cm^{-1}.[44] In contrast to the other structures where the G band has the highest Raman intensity, in qgp the Raman spectrum exhibits peaks at 748 and 964 cm^{-1} whith larger intensities. Also, the C_{20} bcm_{closed} structure has a unique Raman signature at 1945 cm^{-1}, which cannot be confused with the Raman active modes found in other structures. The main Raman peaks of qgp and C_{20} bcm_{closed} are absent in other C_{20} structures and therefore can be used to identify unequivocally these structures in experimental spectra.

IV. CONCLUSIONS

Several C_{20}-based solid structures are proposed, based on first-principles density-functional calculations. The proposed structures are stable against external strain (at least up to 20 GPa) and high temperature (at least to 1000 K). The elastic and electronic properties of the structures are calculated. It is shown, in particular, that fcc, bcc, and sc_{closed} structures manifest the semiconducting properties with the band gap varying from 1.0 to 2.57 eV, while the layered qgp and hcp exhibit metallic conductivity in the in-plane directions. Phonon dispersion curves show the stability of the structures. Calculated Raman spectra can be used for structure identification in experimental studies.

ACKNOWLEDGMENTS

This work was supported by the Academy of Finland through project SA120004 and in the framework of the Center of Excellence Program (2006-2011). We are grateful to Center of Scientific Computing (CSC), Espoo for generous computational resources. The pictures of the molecular structures were drawn using VMD[45] visualization package.

*vehvilainen@iki.fi

[1]Z. Yang, Y. Xia, and R. Mokaya, J. Am. Chem. Soc. **129**, 1673 (2007).
[2]Y.-H. Kim, Y. Zhao, A. Williamson, M. J. Heben, and S. B. Zhang, Phys. Rev. Lett. **96**, 016102 (2006).
[3]Y. Zhao, Y.-H. Kim, A. C. Dillon, M. J. Heben, and S. B. Zhang, Phys. Rev. Lett. **94**, 155504 (2005).
[4]Y. Ren, T. Ng, and K. Liew., Carbon **44**, 397 (2006).
[5]Y. Miyamoto and M. Saito, Phys. Rev. B **63**, 161401 (2001).
[6]S.-H. Ke, H. U. Baranger, and W. Yang, Phys. Rev. Lett. **91**, 116803 (2003).
[7]A. S. Alexandrov, A. M. Bratkovsky, and R. S. Williams, Phys. Rev. B **67**, 075301 (2003).
[8]Y. Tabata and Y. Ikada, Pure Appl. Chem. **71**, 2047 (1999).
[9]W. Noon, Y. Kong, and J. MA, Proc. Natl. Acad. Sci. USA **99**, 6466 (2002).
[10]T. Kyotani, Bull. Chem. Soc. Jpn. **79**, 1322 (2006).
[11]Z. Ma, T. Kyotani, and A. Tomita, Carbon **40**, 2367 (2002).
[12]H. Kroto, J. Heath, S. O'Brien, and R. Smalley, Nature (London) **318**, 162 (1985).
[13]S. Okada and A. Oshiyama, Phys. Rev. B **68**, 235402 (2003).
[14]T. A. Beu, J. Onoe, and A. Hida, Phys. Rev. B **72**, 155416 (2005).
[15]Z. Iqbal, Y. Zhand, H. Grebel, S. Vijayalakshmi, A. Lahamer, G. Benedek, M. Bernasconi, J. Cariboni, I. Spagnolatti, R. Sharma, R. F. J. Owens, M. E. Kozlov, K. V. Rao, and M. Muhammed, Eur. Phys. J. B **31**, 509 (2003).
[16]I. Spagnolatti, M. Bernasconi, and G. Benedek, Europhys. Lett. **59**, 572 (2002).
[17]Z. Wang, X. Ke, Z. Zhu, F. Zhu, M. Ruan, H. Chen, R. Huang, and L. Zheng, Phys. Lett. A **280**, 351 (2001).
[18]Z. Chen, T. Heine, J. Jiao, A. Hirsch, W. Thiel, and P. Schleyer, Chem. Eur. J **10**, 963 (2004).
[19]T. Vehviläinen, J Nanoscience Nanotechnology **9**, 4360 (2009).
[20]S. Okada, Y. Miyamoto, and M. Saito, Phys. Rev. B **64**, 245405 (2001).
[21]G. Kresse and J. Furthmüller, Phys. Rev. B **54**, 11169 (1996).
[22]G. Kresse and J. Furthmüller, Comput. Mater. Sci. **6**, 15 (1996).
[23]J. P. Perdew and Y. Wang, Phys. Rev. B **45**, 13244 (1992).
[24]G. Kresse and D. Joubert, Phys. Rev. B **59**, 1758 (1999).
[25]P. E. Blöchl, Phys. Rev. B **50**, 17953 (1994).
[26]R. Car and M. Parrinello, Phys. Rev. Lett. **55**, 2471 (1985).
[27]CPMD, Copyright IBM Corp 1990-2006, Copyright MPI für Festkörperforschung Stuttgart 1997-2001 (1997-2001).
[28]X. Gonze *et al*., Comput. Mater. Sci. **25**, 478 (2002).
[29]M. Elstner, P. Hobza, T. Frauenheim, S. Suhai, and E. Kaxiras, J. Chem. Phys. **114**, 5149 (2001).
[30]W. T. M. Mooij, F. B. van Duijneveldt, J. G. C. M. van Duijneveldt-van de Rijdt, and B. P. van Eijck, J. Phys. Chem. A **103**, 9872 (1999).
[31]W. T. M. Mooij, B. P. van Eijck, and J. Kroon, J. Phys. Chem. A **103**, 9883 (1999).
[32]R. Williams and D. Malhotra, Chem. Phys. **327**, 54 (2006).
[33]A. A. Ahmadieh and H. A. Rafizadeh, Phys. Rev. B **7**, 4527 (1973).
[34]H. Rydberg, M. Dion, N. Jacobson, E. Schröder, P. Hyldgaard, S. I. Simak, D. C. Langreth, and B. I. Lundqvist, Phys. Rev. Lett. **91**, 126402 (2003).
[35]M. G. Ganchenkova, T. T. Vehviläinen, and R. M. Nieminen, Phys. Rev. B **78**, 195421 (2008).
[36]P. Ravindran, L. Fast, A. Korzhavyi, and B. Johansson, J. Appl. Phys. **84**, 4891 (1998).
[37]F. Murnaghan, Proc. Natl. Acad. Sci. USA **30**, 244 (1944).
[38]H. McSkimi and P. Andreatch, J. Appl. Phys. **43**, 2944 (1972).
[39]I. Spagnolatti, A. Mussi, M. Bernasconi, and G. Benedek, Eur. Phys. J. B **37**, 143 (2003).
[40]S. Baroni, S. de Gironcoli, A. Dal Corso, and P. Giannozzi, Rev. Mod. Phys. **73**, 515 (2001).
[41]X. Gonze and J.-P. Vigneron, Phys. Rev. B **39**, 13120 (1989).
[42]X. Gonze, Phys. Rev. A **52**, 1096 (1995).
[43]X. Gonze and C. Lee, Phys. Rev. B **55**, 10355 (1997).
[44]M. Dresselhaus, G. Dresselhaus, R. Saito, and A. Jorio, Phys. Rep. **409**, 47 (2005).
[45]W. Humphrey, A. Dalke, and K. Schulten, J. Mol. Graphics **14**, 33 (1996).